

Laser-induced fluorescence experimental spectroscopy and theoretical calculations of uranium monoxide

Xi-Lin Bai(白西林), Xue-Dong Zhang(张雪东), Fu-Qiang Zhang(张富强), and Timothy C Steimle
Citation: Chin. Phys. B, 2022, 31 (**5**): 053301. DOI: 10.1088/1674-1056/ac43a4
Journal homepage: http://cpb.iphy.ac.cn; http://iopscience.iop.org/cpb

What follows is a list of articles you may be interested in

Computational design of ratiometric two-photon fluorescent Zn^{2+} probes based on quinoline and di-2-picolylamine moieties

Zhe Shao(邵哲), Wen-Ying Zhang(张纹莹), and Ke Zhao(赵珂)
Chin. Phys. B, 2022, 31 (**5**): 053302. DOI: 10.1088/1674-1056/ac46c6

Laser-induced fluorescence experimental spectroscopy and theoretical calculations of uranium monoxide

Xi-Lin Bai(白西林), Xue-Dong Zhang(张雪东), Fu-Qiang Zhang(张富强), and Timothy C Steimle
Chin. Phys. B, 2022, 31 (**5**): 053301. DOI: 10.1088/1674-1056/ac43a4

Effects of temperature and pressure on OH laser-induced fluorescence exciting A-X (1,0) transition at high pressures

Xiaobo Tu(涂晓波), Linsen Wang(王林森), Xinhua Qi(齐新华), Bo Yan(闫博), Jinhe Mu(母金河), Shuang Chen(陈爽)
Chin. Phys. B, 2020, 29 (**9**): 093301. DOI: 10.1088/1674-1056/aba5ff

Responsive mechanism and coordination mode effect of a bipyridine-based two-photon fluorescent probe for zinc ion

Han Zhang(张瀚), Zhe Shao(邵哲), Ke Zhao(赵珂)
Chin. Phys. B, 2020, 29 (**8**): 083304. DOI: 10.1088/1674-1056/aba9b9

Responsive mechanism and molecular design of di-2-picolylamine-based two-photon fluorescent probes for zinc ions

Mei-Yu Zhu(朱美玉), Ke Zhao(赵珂), Jun Song(宋军), Chuan-Kui Wang(王传奎)
Chin. Phys. B, 2018, 27 (**2**): 023302. DOI: 10.1088/1674-1056/27/2/023302

Laser-induced fluorescence experimental spectroscopy and theoretical calculations of uranium monoxide

Xi-Lin Bai(白西林)[1,†], Xue-Dong Zhang(张雪东)[1], Fu-Qiang Zhang(张富强)[2], and Timothy C Steimle[3]

[1] *School of Physics and Information Engineering, Key Laboratory of Spectral Measurement and Analysis of Shanxi Province, Shanxi Normal University, Linfen* 041004, *China*

[2] *School of Chemical and Material Science, Key Laboratory of Magnetic Molecules & Magnetic Information Materials of Ministry of Education, Shanxi Normal University, Linfen* 041004, *China*

[3] *School of Molecular Science, Arizona State University, Tempe* 85287, *USA*

(Received 19 September 2021; revised manuscript received 7 December 2021; accepted manuscript online 16 December 2021)

As a model molecule of actinide chemistry, UO molecule plays an important role in understanding the electronic structure and chemical bonding of actinide-containing species. We report a study of the laser-induced fluorescence spectra of the $U^{16}O$ and $U^{18}O$ using two-dimensional spectroscopy. Several rotationally resolved excitation spectra were investigated. Accurate molecular rotational constants and equilibrium internuclear distances were reported. Low-lying electronic states information was extracted from high resolution dispersed fluorescence spectra and analyzed by the ligand field theory model. The configuration of the ground state was determined as $U^{2+}(5f^37s)O^{2-}$. The branching ratios, and the vibrational harmonic and anharmonic parameters were also obtained. Radiative lifetimes were determined by recording the time-resolved fluorescence spectroscopy. Transition dipole moments were calculated using the branching ratios and the radiative lifetimes. These findings were elucidated by using quantum-chemical calculations, and the chemical bonding was also analyzed. The findings presented in this work will enrich our understanding of actinide-containing molecules.

Keywords: laser-induced fluorescence, two-dimensional spectroscopy, density functional theory

PACS: 33.20.–t, 31.15.ae, 42.62.Fi **DOI:** 10.1088/1674-1056/ac43a4

1. Introduction

Nuclear power can generate large amounts of energy with low emissions to the atmosphere, making it an attractive alternative to fossil fuels.[1–4] However, it also has some drawbacks, such as long-term storage of nuclear waste and amelioration of existing waste. Uranium monoxide (UO) is an important component in nuclear energy, so the study of UO has contributed to exploring not only the solution of nuclear waste but bonding characteristics and electronic structure of actinides. UO gas-phase molecule provides the most direct experimental method to clarify the bonding properties, especially when combined with theoretical models. However, considering that the uranium element has an open f orbital, UO has many low-energy electronic states and has a strong relativistic effect.[5–7] Coupled with the experimental dangerous and expensive costs, as well as the complexity of theoretical calculations, there are still huge challenges to the research on UO both experimentally and theoretically. Laser-induced fluorescence (LIF) technology combined with density functional theory (DFT) calculation[6,8–11] happens to be a powerful technology for studying the electronic vibration and spin-orbit[12] of the target molecule.

The initial experimental report on UO spectroscopy was infrared spectra[13,14] recorded in argon and neon matrices, and the vibrational frequency was obtained. The first report on the electronic spectrum[15–18] for gas-phase UO was performed using two-color resonance-enhanced photoionization experiments. Immediately, further analysis and identification of the UO spectrum was completed by Kaledin *et al.*[19] The spectral constants and good quantum number, Ω'', of the electron ground state were confirmed. The electric dipole moments, and magnetic g factors for UO were determined by measuring optical Stark and Zeeman spectra,[20] respectively. The electronic and vibrational structures of UO were investigated using high-resolution photoelectron imaging. Further, on the theoretical side, there are also discussions on the structure and spectroscopic properties of UO. However, the inaccurate research results, especially the vibrational frequency, indicate the need for careful investigation of the electronic structure and chemical bonding of UO.

In this article, the high resolution LIF spectra of $U^{16}O$ and $U^{18}O$ in the range of 16000 cm^{-1}–19000 cm^{-1}, using two-dimensional (2D) spectroscopy,[21–24] were recorded and rotationally analyzed. Rotation-resolved spectroscopy demonstrates that the ground state is clearly characterized as $\Omega'' = 4$. In addition to studying several electronic states previously studied, this work also discovered a new electronic state located at 18056.58 cm^{-1}. By measuring the higher resolution dispersed fluorescence (DF) spectra, accurate low-lying electronic vibrational states, vibrational frequencies, and fluorescence branching ratios can be procured. The transition dipole moment can also be obtained by combining the fluorescence

†Corresponding author. E-mail: bxl5630@mail.ustc.edu.cn

© 2022 Chinese Physical Society and IOP Publishing Ltd

lifetime and branching ratios. Finally, the geometric configuration, bonding orbitals analysis, vibrational frequency, permanent dipole moment, and bond order were performed using high-level *ab initio* calculations to provide a better understanding of the electronic structure and chemical bonding of UO.

2. Experimental and computational methods

2.1. Experimental methods

Details of the experimental setup for recording laser-induced fluorescence spectra have been described in our previous studies. An internally cold $U^{16}O$ and $U^{18}O$ molecular beams were produced using laser ablation on a rotating uranium rod in a supersonic expansion of 2% O_2 gas mixture seeded in helium and 1% $^{18}O_2$ gas mixture seeded in helium at a same stagnation pressure of ~ 2 MPa. After the UO molecular beams were excited by the pulsed dye laser, the fluorescence signals could be obtained using the two-dimensional spectroscopic technique.[21–25] In brief, the 2D spectra were built by scanning the wavelength of the pulsed dye laser and capturing the dispersed laser-induced fluorescence (DLIF) by a monochromator with a low f-number value. The final signal was visualized using a cooled, gated, intensified charge coupling device (CCD). In this experiment, the ablation laser (355 nm, $\sim$ 20 mJ/pulse, 20 Hz) was focused by a plane-convex lens and then interacted with the molecular beam, a pulsed dye laser using C503, C540A, and R590 dyes was pumped by an Nd:YAG laser (355 nm, $\sim$ 50 mJ/pulse, 20 Hz) to generate a continuously tunable wavelength region between 500 nm and 600 nm. Two digital delay pulse generators were used to control the timing sequence of the pulsed nozzle, the ablation and excitation lasers, and CCD.

In addition to recording 2D spectra, higher resolution dispersed fluorescence spectra and the lifetime measurements of the excited states can also be obtained using this experimental setup. By selecting the wavelength of the pulsed excitation laser and narrowing the entrance slit of the monochromator, higher resolution DF spectra were obtained. In general, ten thousand laser pulses are required to obtain higher resolution DLIF spectra. The relative sensitivity of the detector ICCD and the wavelength of DLIF spectra were calibrated by the blackbody radiation method and the emission of argon pen lamp, respectively. The time-resolved fluorescence spectroscopy was measured by recording the DF spectra under a gradually changing time delay of the CCD relative to the pulsed dye laser. The radiation lifetimes[26–29] of the excited states could be finally determined by fitting the time-resolved fluorescence spectroscopy.

2.2. Computational methods

In this study, we used the DFT method to calculate the geometric configuration, vibrational frequency, bond order, and permanent dipole moment of the ground state of UO.[30] In order to better understand the chemical bonding characteristics of UO, a detailed analysis was carried out from the perspectives of natural bond orbital (NBO) theory.[31–34] According to the previous DFT calculation experience, the generalized gradient approximation (GGA)[35] in conjunction with the exchange-correlation functional PBE and the Slater's-type TZ2P basis set[36–40] can be used to obtain relatively accurate calculation results. Under the premise of not affecting the calculation accuracy, the frozen core approximation was applied to the [$1s^2$–$5d^{10}$] for U and [$1s^2$] for O to save computational time.[41] Considering the relativistic effect, zero-order regular approximation (ZORA) and the exact two-component (X2C) relativistic hamiltonian were adopted according to the requirements of the calculation task. The accuracy of X2C is slightly higher than that of ZORA, due to major advances in the relativistic hamiltonian. Considering the amount of calculation, we only use it for the calculation of orbital components and permanent dipole moments. Among them, the scalar relativistic-ZORA (SR-ZORA) method was used in geometry optimization to deal with the scalar relativistic effect. Subsequently, based on the geometric configuration optimized by SR-ZORA, the molecular vibrational frequency was obtained by calculating the infrared spectrum of the ground state. And, the spin–orbit coupled ZORA (SO-ZORA) method was used to consider the spin–orbit coupling effect. It is worth noting that in order to obtain a more accurate electronic structure when calculating the vibrational frequency, the frozen core approximation was abandoned. Finally, on the basis of the functional and basis set unchanged, the frozen core approximation was canceled, and the SR-ZORA and X2C relativistic effects were considered to calculate the permanent dipole moments, the orbital bonding, and bond order analysis of UO through single-point energy calculations.

3. Results and discussion

3.1. Rotational analyses of the observed bands

In the experiment methods described in the preceding text, the 2D spectra were obtained by simultaneously recording the wavelength of the monochromator relative to the laser excitation wavelength. Figure 1 presents the 2D spectrum obtained by scanning the excitation laser in the range of 17500 cm^{-1}–17700 cm^{-1}. The horizontal axis displays the wavenumber of the excitation laser, and the vertical axis displays the wavelength of the dispersed fluorescence. The excitation spectra shown at the top of the 2D spectrum are generated by the vertical integration of a horizontal slice (marked in red). From left to right: the bands of UO at [17.521], [17.547], [17.614], and [17.654] are labeled as $[18.403]5/[18.404]5(v=1)-X(1)4(v=1)$, $[18.430]5(v=1)-X(1)4(v=1)$, $[17.614]5-X(1)4$, and $[17.654]5(v=$

1) – X(1)4, respectively. They are low-resolution LIF spectra of UO obtained by recording the off-resonance emission. The dispersed LIF spectrum displayed at the right hand side of the 2D spectrum is generated by horizontally integrating the vertical slices (marked in green). This is the low-resolution DLIF spectrum of the band near 17614 cm^{-1}. Figure 2 presents another 2D spectrum in the range of 18020 cm^{-1}–18220 cm^{-1}. The excitation spectra are presented at the top of the 2D spectrum. From left to right: the bands of UO at [18.056], [18.110], and [18.136] are labeled as [18.056]3 – X(1)4, [18.403]5/[18.404]5($v = 1$) – (2)4, and [18.430]5($v = 1$) – (2)4, respectively. The dispersed LIF spectrum shown at the right hand side of the 2D spectrum is the band near 18056 cm^{-1}.

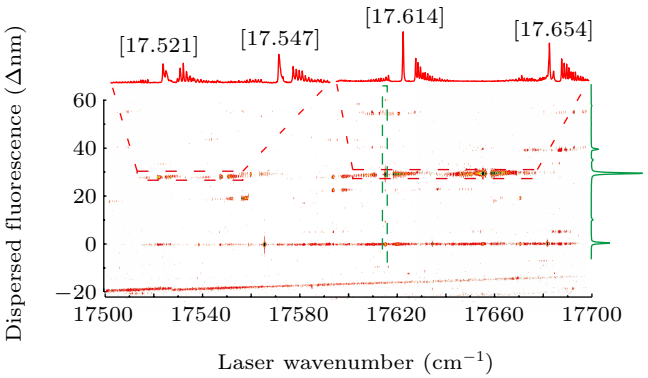


Fig. 1. The 2D spectrum of UO in the range from 17500 cm^{-1} to 17700 cm^{-1}.

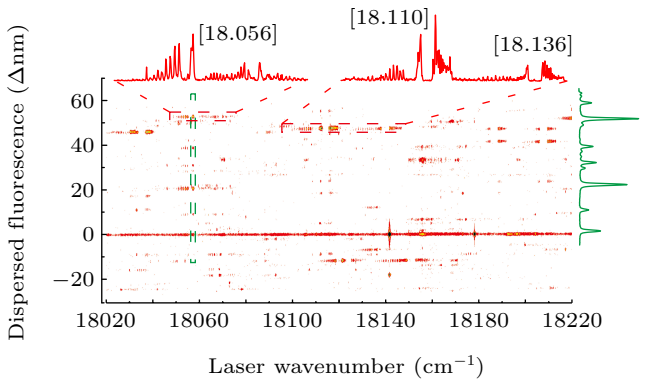


Fig. 2. The 2D spectrum of UO in the range from 18020 cm^{-1} to 18220 cm^{-1}.

The experimental laser excitation spectrum band near 17614 cm^{-1} displayed in the upper panel of Fig. 3, which is labeled as [17.614]5 – X(1)4, was selected for rotational analysis. The simulated spectrum, displayed in the lower panel of Fig. 3, was fitted by using the PGOPHER program. The good resolution of $P(J)$ and $R(J)$ branches allows us to assign all transitions. The simulation was completed under the conditions of a rotation temperature of 40 K, a Gaussian linewidth of 0.2 cm^{-1}, and the assumption that the upper and lower states were Hund's case (c) angular momentum coupling. The fitting was performed using the following simplified equation:

$$\begin{aligned} \nu = \nu_0 + \left[B'J'(J'+1) - B''J''(J''+1)\right] \\ - \left[D'J'(J'+1) - D''J''(J''+1)\right], \end{aligned} \quad (1)$$

where ν_0 is the band origin, B is the rotational constant, and D is the centrifugal distortion constant. Through the identification, we can see that for the stronger $R(J)$ branch, the minimum J value is 4; for the weaker $P(J)$ branch, the minimum J value is 6. Based on these characteristics, this band is identified as [17.614]5 – X(1)4. This assignment supports evidence of the previous research by Kaledin *et al.*[19] The only difference is that they obtained the spectrum at high temperature, while we are at low temperature, so their rotational population is higher than our experimental results. In addition, the rotational constant of 0.33611 cm^{-1} for the ground state through fitting is also in accord with their measurement. The quantitative molecular parameters were obtained from the fitting are listed in Table 1. Strangely, we can see that the location of the P branch fits better, but the intensity deviation is large from Fig. 3. This phenomenon also occurs in uranium-containing compounds that we have previously studied. The main reason for the intensity difference is that we choose the main component to fit in PGOPHER fitting. However, the molecular configuration and bonding relationship of UO molecule are more complicated due to the open f and d orbitals.

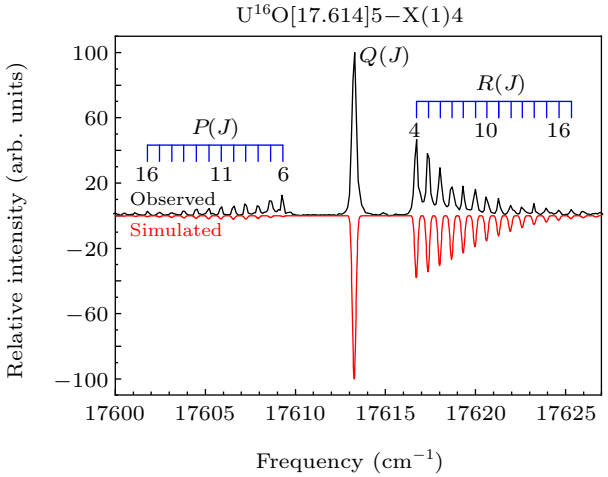


Fig. 3. Rotationally resolved spectrum of the [17.614]5 – X(1)4 band of UO. The upper trace is the experimental spectrum, and the lower trace is the simulated spectrum.

The high-resolution rotational spectra of the isotopomer $U^{18}O$ were also studied in our experiment. The isotopomer $U^{18}O$ band at 17632 cm^{-1}, which is similar to the $U^{16}O$ band at 17614 cm^{-1} ([17.614]5 – X(1)4 transition), was shown in Fig. 4. It can be seen that the R branch is stronger than the P branch, which conforms to the transition characteristic of $\Delta\Omega = 1$. Consistent with the above identification method, the upper state of the 17632 cm^{-1} state was marked as $\Omega' = 5$, and the lower state was marked as $\Omega'' = 4$. The molecular rotational constant of the ground state is determined to

be 0.29403 cm^{-1}, it is in good agreement with the value determined by Kaledin *et al.*[19,42] The determined molecular constants for $U^{18}O$ bands are shown in Table 1. The $U^{16}O$ band at 17614 cm^{-1} is the strongest band in the region of 17500 cm^{-1}–17700 cm^{-1}. For the isotopomer $U^{18}O$ spectrum, there are only two stronger bands in this region, namely the $U^{18}O$ band at 17632 cm^{-1} and 17567 cm^{-1}. The sharp $Q(J)$ branches of those two bands and the similar rotational constants for upper and lower states imply that the 0–0 bands dominate the spectra. From the shape of the spectrum, the $U^{18}O$ band at 17632 cm^{-1} was determined to be an isotopic companion of the $U^{16}O$ band at 17614 cm^{-1}. In the absence of perturbation, the isotope shift between similar potential energy curves is very small. The large isotope shift means that there may be perturbations in the electronic state, leading to more significant changes in the UO energy level. The absence of strong vibrational progressions also supports this view in Kaledin's research.[19] The perturbation may come from the interaction of the dark state and the bright state.

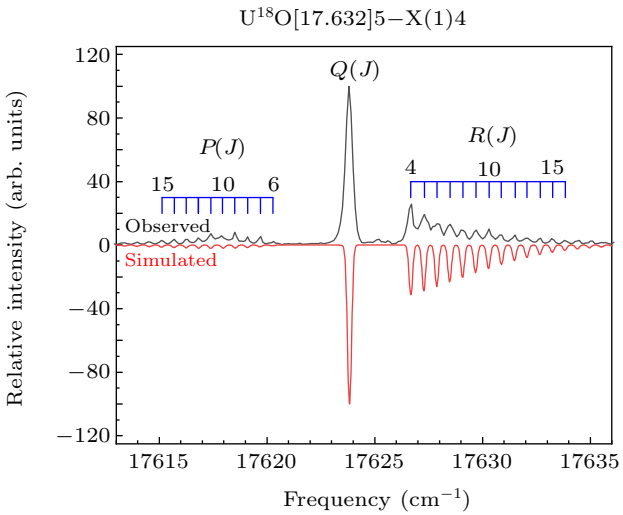


Fig. 4. Rotationally resolved spectrum of the [17.632]5 – X(1)4 band of $U^{18}O$. The upper trace is the experimental spectrum, and the lower trace is the simulated spectrum.

Table 1. Equilibrium molecular parameters of $U^{16}O$ and $U^{18}O$ for selected Ω states.

Molecule	State	PGOPHER		Combination differences	
		B_0 (cm^{-1})	Re (Å)	B_0 (cm^{-1})	Re (Å)
$U^{16}O$	X(1)4	0.33611	1.82870	0.33574	1.82971
	(1)4($v=1$)	0.33211	1.83968	0.33095	1.84290
	(2)4($v=0$)	0.34657	1.80089	0.34653	1.80100
	[17.614]5($v=0$)	0.33439	1.83340	0.33367	1.83537
	[17.653]5($v=1$)	0.33548	1.83042	0.33292	1.83744
	[18.056]3(v)	0.32999	1.84558	0.32990	1.84583
	[18.403]5(v)	0.33070	1.84360	0.33064	1.84376
	[18.404]5($v=1$)	0.33822	1.82299	0.33885	1.82129
	[18.430]5($v=1$)	0.33235	1.83902	0.33264	1.83821
$U^{18}O$	X(1)4	0.29909	1.83497	0.29959	1.83344
	[17.567]5	0.29750	1.83987	0.29753	1.83977
	[17.632]5	0.29803	1.83823	0.29947	1.83381

Note: the errors obtained by PGOPHER and combination differences are 2% and 3%, respectively.

In the two spectral ranges of 17500 cm^{-1}–17700 cm^{-1} and 18020 cm^{-1}–18220 cm^{-1}, in addition to several transitions described above, there are several transitions of [18.403]5(v)/[18.404]5($v=1$)-X(1)4($v=1$)/(2)4($v=0$), [18.430]5($v=1$)-X(1)4($v=1$)/(2)4($v=0$). The rotational constants obtained by fitting these bands are also listed in Table 1. It can be seen from the spectral shape that the Q branch of the corresponding spectrum in the lower state of X(1)4($v=1$) is narrower than that in the state of (2)4($v=0$). This is because the equilibrium internuclear distances of the upper and lower states of the former spectrum are consistent while that of the latter are different, which also indicates that the configurations of X(1)4($v=1$) and (2)4($v=0$) states are inconsistent. We will analyze below that these two states are derived from different electronic configurations. Compared to previous studies, a new $U^{16}O$ band located at 18056.58 cm^{-1} was also discovered. Through the analysis of the high-resolution rotational spectrum, it is found that the $P(J)$ branch of the spectrum is extremely strong, while the $R(J)$ branch is very weak, which is in line with the transition characteristics of $\Delta\Omega=-1$. Through spectral fitting, we attribute this band to the transition of [18.056]3 – X(1)4, and the rotational constant of the [18.056]3 state is 0.32999 cm^{-1}.

Considering that there may be perturbations in the upper states, we use the combined differences method to obtain the rotational constants. This method can effectively eliminate the perturbation influence from the upper states. The differences between the low J lines can be directly obtained by the experimental spectrum. Then the ground state rotational constant B'' can be determined by

$$R(J-1)-Q(J)=2JB'', \tag{2}$$

$$R(J-1)-P(J+1)=(4J+2)B'', \tag{3}$$

$$Q(J)-P(J+1)=(2J+2)B''. \tag{4}$$

The ground state rotational constant obtained using this method is 0.33574 cm^{-1}, which seems to be consistent with the value obtained by fitting the experimental spectrum. The band origin ν_0 and the upper state rotational constant B' also can be calculated using this method. The rotational constants of the [17.614]5 and [18.056]3 states of $U^{16}O$ and the [17.632]5 state of $U^{18}O$ are 0.33367 cm^{-1}, 0.32990 cm^{-1}, and 0.29947 cm^{-1}, respectively. The rotational constants of the above three states are obtained by spectral fitting as 0.33439 cm^{-1}, 0.32999 cm^{-1}, and 0.29403 cm^{-1}, respectively. The rotational constants obtained from both approaches are well matched and listed in Table 1. We speculate that the perturbation has little effect on the molecular constants of the upper state.

Table 2. Calculated natural bond orbital compositions of $U^{16}O$ and $U^{18}O$ based on ADF/PBE/TZ2P calculations.

Molecule	Composition	U % 7s	U % 6d	U % 5f	U % 7p	O % 2s	O % 2p
$U^{16}O$	U–^{16}O π		7.07	5.67			87.13
	U–^{16}O π	0.05	8.38	6.76	0.14	4.01	80.47
	U–^{16}O σ	0.11	10.06	8.17	0.32	8.86	72.27
$U^{18}O$	U–^{18}O π		7.18	5.56		0.29	86.82
	U–^{18}O π	0.01	7.42	5.91	0.03	0.92	85.56
	U–^{18}O σ	0.13	10.88	8.97	0.04	11.7	67.68

To better understand the chemical bonding and electronic structures of UO, high level *ab initio* calculations on the ground state for $U^{16}O$ and $U^{18}O$ were performed. The calculated equilibrium bond lengths of ground states for $U^{16}O$ and $U^{18}O$, based on ADF/PBE/TZ2P, are both 1.847 Å, which is consistent with the calculated results by Zhou *et al.*[43] In the experiment, we also obtained the equilibrium bond lengths through the rotational constants, which are also identical with the calculated values. The calculated natural bond orbital compositions of $U^{16}O$ and $U^{18}O$ based on ADF/PBE/TZ2P are shown in Table 2. The results indicate there are one σ bond and two π bonds in the UO molecule. It can be seen from Table 2 that most of the constituents of the bonding molecular orbitals are derived from the O-2p atomic orbital, and the contribution from the O-2p atomic orbital in the π-bonded molecular orbital is as high as 87%, so the effective bond orders of UO should not reach 3. Through the calculation of the bond order, the accuracy of the above-mentioned orbital bonding analysis can be verified. For $U^{16}O$, the calculated Mayer and the G–J bond orders are both near 2. The calculated G–J and Mayer bond orders are 2.400 and 2.122, respectively, which are consistent with the value of 2.37 calculated by Li *et al.*[30] Generally, the bond order of $U^{16}O$ should be equal, or approximately equal, to the bond order of $U^{18}O$. For $U^{18}O$, the calculated G–J and Mayer bond orders are 2.397 and 2.120, respectively. Moreover, the agreement of the bond-order calculation results also indicates that the bond length of the ground state of $U^{16}O$ is basically the same as that of $U^{18}O$. The results are in keeping with previous experimental studies,[41] in which the ground state equilibrium bond lengths of $U^{16}O$ and $U^{18}O$ are almost identical. According to the calculated results of the natural bond orbital theory and the bond order, it is shown that the UO molecular bond has the characteristics of multiple bonds.

3.2. Low-lying electronic states

To better study the low-lying electronic states, the $[18.056]3-X(1)4$ band with abundant fluorescence information was analyzed. Figure 5 shows the high-resolution dispersed fluorescence spectrum obtained by exciting the Q-head in the $[18.056]3-X(1)4$ band. The wavelength and intensity of the DF spectrum were calibrated by argon pen lamp and black body radiation, respectively. The associated energy levels relative to ground state zero-point levels are presented and the observed dispersed fluorescence features are assigned. Using the ligand field theory (LFT) model, several low-lying electronic vibrational energy levels can be well identified. The energy of the vibration terms of the low-lying electronic states, listed in Table 3, is extracted from the high-resolution dispersed fluorescence spectrum. In order to facilitate the comparison, the previous results are also listed. The vibrational harmonic and anharmonic parameters ω_e and $\omega_e x_e$, were obtained by fitting the simple harmonic oscillator equation

$$G_{v''} = \omega_e''(v''+1/2) - \omega_e x_e''(v''+1/2)^2, \tag{5}$$

the harmonic vibrational frequency $\omega_e = 845.4$ cm^{-1} and the anharmonicity constant $\omega_e x_e = 2.5$ cm^{-1} of $U^{16}O$ were determined using the method of least squares. The determined values are consistent with the values of $\omega_e = 846.5$ cm^{-1} and $\omega_e x_e = 2.3$ cm^{-1} measured by Kaledin *et al.*[19]

Table 3. Constants for the low-lying states of $U^{16}O$ and $U^{18}O$ (in unit cm^{-1}).

State	UO, this work	UO, exp^{Heaven}	$U^{18}O$, this work
X(1)4 ($v=0$)	0	0	0
X(1)4 ($v=1$)	880	882	837
X(1)4 ($v=2$)	1733	1734	1655
X(1)4 ($v=3$)	2567	2569	
(2)4 ($v=0$)	294	294	290
(2)4 ($v=1$)	1186	1184	1129
(1)3 ($v=0$)	651	651	
(1)3 ($v=1$)	1493		
(1)2 ($v=0$)	961	959	
(1)2 ($v=1$)	1801		
(1)5 ($v=0$)	1046	1043	
(1)5 ($v=1$)	1894	1885	
(1)5 ($v=2$)	2720		
(3)4 ($v=0$)	1578	1574	
(3)3 ($v=0$)	1937	1941	

The LFT model predicts that the states derived from the same electronic configuration will have similar vibrational frequencies and rotational constants. Previous studies demonstrated that there are two configurations $(U^{2+}(5f^37s)O^{2-}$ and

$U^{2+}(5f^27s^2)O^{2-}$) in the low-lying states of UO. The rotational constant of ground state X(1)4 state for $U^{16}O$ is 0.33611 cm^{-1}, and the rotational constant of the X(2)4 state is 0.34657 cm^{-1}. The electrons on the 5f and 7s orbitals have different shielding effects, the state in the $5f^37s$ configuration has lower vibrational frequencies and smaller rotational constants than the state in the $5f^27s^2$ configuration. As a result, the X(1)4 and X(2)4 states are derived from the configuration $U^{2+}(5f^37s)O^{2-}$ and configuration $U^{2+}(5f^27s^2)O^{2-}$, respectively. The above analysis has determined that the harmonic vibrational frequency of the ground state X(1)4 is 845.4 cm^{-1}. However, for the X(2)4 state, only the vibrational energy level $v = 0$, 1 was observed, so the vibrational frequency and anharmonicity constant of this state cannot be determined. Therefore, the electronic configuration cannot be distinguished based on the vibrational frequency.

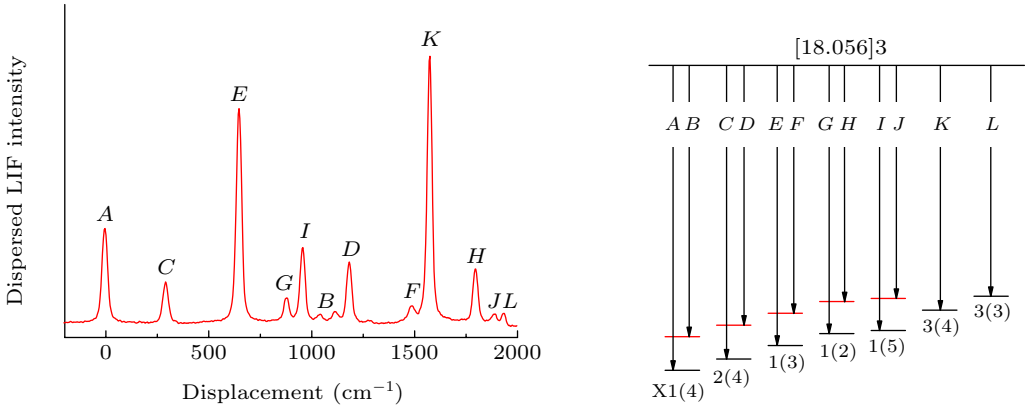


Fig. 5. The dispersed fluorescence spectrum obtained by exciting the Q-branch of the $[18.056]3 - X(1)4$ ($T_v = 18056$ cm^{-1}) band of UO and the corresponding assignment.

It is known that the rotational constants of $U^{16}O$ and $U^{18}O$ are 0.33611 cm^{-1} and 0.29909 cm^{-1}, respectively, and then the equilibrium internuclear distance can be determined. The results show that the equilibrium internuclear distance is nearly equal. The calculated vibrational frequencies of $U^{16}O$ and $U^{18}O$ based on ADF/PBE/TZ2P are 850 cm^{-1} and 804 cm^{-1}, respectively. The calculated vibrational frequency values agree well with the estimated values by the reduced mass and the experimental data. Unfortunately, the experimental spectrum of $U^{18}O$ contains strong interference from $U^{16}O$ signal, and we have not been able to complete the analysis of the low-lying electronic states of $U^{18}O$. According to the above analysis, for $U^{18}O$, its ground state configuration should be $U^{2+}(5f^37s)O^{2-}$, which is the same as $U^{16}O$, because it has almost the same equilibrium internuclear distance.

The charge population and spin density analysis of the ground state for UO was carried out based on ADF/PBE/TZ2P, and the analysis results were shown in Table 4. The charge population results indicate that the uranium atom always loses electrons and becomes an electron donor, and the oxygen atom always gains electrons and becomes an electron acceptor. This characteristic can also be confirmed by electronegativity. The electronegativity of oxygen atom is 3.44, which is much greater than that of uranium atom, which is 1.70. Therefore, oxygen atom can easily obtain electrons from uranium atom. The charge population results indicate that there are hybrid orbitals mixing 5f, 6d, and 7s orbitals of uranium with the 2p orbital of oxygen in UO molecule. Obvious orbital hybridization and orbital mixing calculation results demonstrate that the bonding strength of U–O bond is quite strong. Furthermore, the spin density results indicate that the uranium atom has a positive contribution to the total spin multiplicities of UO, while the oxygen atom has a negative contribution.

Table 4. Population properties for $U^{16}O$ and $U^{18}O$ molecules.

Molecule	Atom	Charge	Spin density
$U^{16}O$	U	0.6693	4.1149
	O	−0.6693	−0.1149
$U^{18}O$	U	0.6697	4.1161
	O	−0.6697	−0.1161

3.3. Radiative lifetimes and transition dipole moments

The experimentally determined radiative lifetime, $\tau_{iv'}$, for the [18.056]3 state is 266(11) ns which was determined by fitting the time-resolved fluorescence spectrum to a single exponential function. Combined with the branching ratios obtained by the DF spectrum, the magnitude of the vibrational transition dipole moments can be calculated by

$$A_{iv',fv''} = 3.136 \times 10^{-7} \left|\mu_{iv',fv''}\right|^2 \nu^3_{iv',fv''} = b_{iv',fv''} \tau^{-1}_{iv'}, \quad (6)$$

where $A_{iv',fv''}$ is the Einstein spontaneous emission coefficient, $\mu_{iv',fv''}$ is the vibronic transition dipole moment, and $b_{iv',fv''}$ is the fluorescence branching ratio. The fluorescence branch ratios can be obtained by calibrating the intensity of DF spectrum in Fig. 5 and integrating the peak area, and then combining the experimentally measured radiation lifetimes to calculate the vibronic transition dipole moments $\mu_{iv',fv''}$.

Table 5. The transition wavenumbers (in unit cm^{-1}), energies (in unit cm^{-1}), branching ratios (%), and vibrational transition dipole moments (in unit D) of the dispersed fluorescence spectra obtained by exciting the Q-branch of the $[18.056]3-X(1)4$ transition of UO.

Band	Excited state: [18.056]3				
	Assignment	Trans[a]	Energy[a]	BR[b]	Td[b]
A	$[18.056]3 \rightarrow X(1)4\ (v=0)$	18056	0	12.08	0.50
B	$[18.056]3 \rightarrow X(1)4\ (v=1)$	17716	880	0.97	0.14
C	$[18.056]3 \rightarrow (2)4\ (v=0)$	17762	294	5.43	0.34
D	$[18.056]3 \rightarrow (2)4\ (v=1)$	16870	1186	7.15	0.42
E	$[18.056]3 \rightarrow (1)3\ (v=0)$	17405	651	25.13	0.76
F	$[18.056]3 \rightarrow (1)3\ (v=1)$	16563	1493	1.76	0.22
G	$[18.056]3 \rightarrow (1)2\ (v=0)$	17095	961	3.00	0.27
H	$[18.056]3 \rightarrow (1)2\ (v=1)$	16255	1801	6.32	0.42
I	$[18.056]3 \rightarrow (1)5\ (v=0)$	17010	1046	8.39	0.45
J	$[18.056]3 \rightarrow (1)5\ (v=1)$	16162	1894	1.12	0.18
K	$[18.056]3 \rightarrow (3)4\ (v=0)$	16478	1578	27.82	0.86
L	$[18.056]3 \rightarrow (3)3\ (v=0)$	16119	1937	0.83	0.15

[a]The estimated uncertainty of the transition wavenumbers and the energy of the lower state is $\pm 10\ cm^{-1}$.

[b]The errors of branching ratios and transition dipole moments are ±5%.

According to the DF spectrum calibrated by intensity and wavelength, the observed transition wavenumbers, corresponding energies, fluorescence branch ratios, and the vibronic transition dipole moments $\mu_{iv',fv''}$ of the [18.056]3 state are shown in Table 5. In addition, the calculated permanent electric dipole moments of $U^{16}O$ and $U^{18}O$ at the ADF/PBE/TZ2P level are 3.365 D and 3.363 D, respectively. These findings support the result that the obtained $U^{16}O$ permanent electric dipole moment value was 3.363 D using Zeeman spectroscopy experiments by Heaven *et al.*[44]

4. Conclusion and perspectives

In conclusion, we have obtained the 2D (excitation and dispersed fluorescence) spectra of $U^{16}O$ and $U^{18}O$ and explained it using quantum-chemistry calculation. The rotational constants, equilibrium internuclear distances, electron configurations, and vibrational frequencies of the ground state of $U^{16}O$ have been investigated. Laser-induced dispersed fluorescence spectra of the $[17.614]5-X(1)4$ for $U^{16}O$, $[17.632]5-X(1)4$ for $U^{18}O$ bands were studied. Many low-lying excited states have been characterized by the LFT model. Radiative lifetimes and branching ratios were measured and used to calculate the transition dipole moments. High-level *ab initio* calculations explained the experimental spectra well, natural orbital analysis and bond order calculations promote a comprehensive understanding of the electronic structure and chemical bonding of UO. Our research provides accurate geometric structure and electronic structure information, which will provide benchmark support for the subsequent actinide chemical calculations.

Acknowledgments

We thank Dr. Anh T. Le (School of Molecular Sciences, Arizona State University) for her technical assistance and helpful discussion. Project supported by the National Natural Science Foundation of China (Grant No. 21903050).

References

[1] Yasuoka H, Koutroulakis G, Chudo H, Richmond S, Veirs D K, Smith A I, Bauer E D, Thompson J D, Jarvinen G D and Clark D L 2012 *Science* **336** 901
[2] Petrović J, Göök A and Cederwall B 2021 *Sci. Adv.* **7** eabg3032
[3] Herzberg R D, Greenlees P T, Butler P A, *et al.* 2006 *Nature* **442** 896
[4] Burns P C, Ewing R C and Navrotsky A 2012 *Science.* **335** 1184
[5] Kovács A, Konings R J M, Gibson J K, Infante I and Gagliardi L 2015 *Chem. Rev.* **115** 1725
[6] Lei S Y, Zhong J, Zhou D L, Zhu F Y and Deng C X 2017 *Chin. Phys. B* **26** 117001
[7] Urban M, Noga J, Cole S J and Bartlett R J 1985 *J. Chem. Phys.* **83** 4041
[8] Parlinski K and Piekarz P 2021 *J. Raman Spectrosc.* **52** 1346
[9] Malyshev A V., Glazov D A, Kozhedub Y S, Anisimova I S, Kaygorodov M Y, Shabaev V M and Tupitsyn I I 2021 *Phys. Rev. Lett.* **126** 183001
[10] Tong Y X, Zhang Q H and Gu L 2018 *Chin. Phys. B* **27** 066107
[11] Pluengphon P, Tsuppayakorn-aek P, Inceesungvorn B, Pinsook U and Bovornratanaraks T 2021 *Mater. Chem. Phys.* **267** 124708
[12] Zhang L, Zou W, Yu Y, Zhao D, Ma X and Yang J 2021 *J. Quantum Spectrosc. Radiat. Transfer* **269** 107690
[13] Gabelnick S D, Reedy G T and Chasanov M G 1973 *J. Chem. Phys.* **58** 4468
[14] Green D W, Reedy G T and Gabelnick S D 1980 *J. Chem. Phys.* **73** 4207
[15] Czekner J, Lopez G V and Wang L S 2014 *J. Chem. Phys.* **141** 244302
[16] Yun Y, Legut D and Oppeneer P M 2012 *J. Nucl. Mater.* **426** 109
[17] Hunt R D and Andrews L 1993 *J. Chem. Phys.* **98** 3690
[18] Elorrieta J M, Bonales L J, Baonza V G and Cobos J 2018 *J. Nucl. Mater.* **503** 191
[19] Kaledin L A, Mccord J E and Heaven M C 1994 *J. Mol. Spectrosc.* **164** 27
[20] Heaven M C, Goncharov V, Steimle T C, Ma T and Linton C 2006 *J. Chem. Phys.* **125** 204314
[21] Gascooke J R, Alexander U N and Lawrance W D 2011 *J. Chem. Phys.* **134** 184301
[22] Gascooke J R and Lawrance W D 2013 *Chem. Phys. Lett.* **555** 38
[23] Gascooke J R, Alexander U N and Lawrance W D 2012 *J. Chem. Phys.* **136** 134309
[24] Reilly N J, Schmidt T W and Kable S H 2006 *J. Phys. Chem. A* **110** 12355
[25] Bai X L and Steimle T C 2020 *Astrophys. J.* **889** 147
[26] Kokkin D L, Steimle T C and Demille D 2014 *Phys. Rev. A* **90** 062503
[27] Mandal P K, Das R C, Seema A U, Sahoo A C, Shah M L, Pulhani A K, Manohar K G and Dev V 2014 *Appl. Phys. B* **116** 407

[28] Sanli A, Pan X, Beecher D S, Magnier S, Lyyra A M and Ahmed E H 2019 *J. Mol. Spectrosc.* **355** 1
[29] Bouchard J L, Steimle T C, Kokkin D L, Sharfi D J and Mawhorter R J 2016 *J. Mol. Spectrosc.* **325** 1
[30] Li P, Jia T T, Gao T and Li G 2012 *Chin. Phys. B* **21** 043301
[31] Mulliken R S 1962 *J. Chem. Phys.* **36** 3428
[32] Reed A E, Curtiss L A and Weinhold F 1988 *Chem. Rev.* **88** 899
[33] Lia Fonseca Guerra C, Handgraaf J, Jan Baerends E and Matthias Bickelhaupt F 2004 *J. Comput. Chem.* **25** 189
[34] Hirshfeld F L 1977 *Theor. Chim. Acta* **44** 129
[35] Perdew J P, Burke K and Ernzerhof M 1996 *Phys. Rev. Lett.* **77** 3865
[36] Skripnikov L V and Titov A V 2015 *J. Chem. Phys.* **142** 024301
[37] Stephens P J, Devlin F J, Chabalowski C F and Frisch M J 1994 *J. Phys. Chem.* **98** 11623
[38] Becke A D 1993 *J. Chem. Phys.* **98** 5648
[39] Van Lenthe E and Baerends E J 2003 *J. Comput. Chem.* **24** 1142
[40] Velde G T, Bickelhaupt F M, Baerends E J, Guerra C F, Snijders J G and Ziegler T 2001 *J. Comput. Chem.* **22** 931
[41] Li Y L, Zou J H, Xiong X G, Su J, Xie H, Fei Z J, Tang Z C and Liu H T 2017 *J. Phys. Chem. A* **121** 2108
[42] Laatiaoui M, Lauth W, Backe H, *et al.* 2016 *Nature* **538** 495
[43] Zhou M F, Andrews L, Ismail N and Marsden C 2000 *J. Phys. Chem. A* **104** 5495
[44] Heaven M C, Nicolai J P, Riley S J and Parks E K 1985 *Chem. Phys. Lett.* **119** 229